Ethylene plays a dual role in sex determination and fruit shape in cucurbits

Adnane Boualem, Serge Berthet, Ravi Sureshbhai Devani, Celine Camps, Sebastien Fleurier, Halima Morin, Christelle Troadec, Nathalie Giovinazzo, Nebahat Sari, Catherine Dogimont, et al.

Ethylene plays a dual role in sex determination and fruit shape in cucurbits.

Adnane Boualem[1], Serge Berthet[1], Ravi Sureshbhai Devani[1], Celine Camps[1], Sebastien Fleurier[1], Halima Morin[1], Christelle Troadec[1], Nathalie Giovinazzo[2], Nebahat Sari[2], Catherine Dogimont[2] and Abdelhafid Bendahmane[1*]

[1] Université Paris-Saclay, CNRS, INRAE, Univ Evry, Institute of Plant Sciences Paris-Saclay (IPS2), 91190, Gif sur Yvette, France.

[2] INRAE GAFL, Génétique et Amélioration des Fruits et Légumes, 84143, Montfavet, France.

Twitter handle : @AdnaneBoualem

*Lead Contact: abdelhafid.bendahmane@inrae.fr

Summary

Shapes of vegetables and fruits are the result of adaptive evolution and human selection. Modules controlling organ shape have been identified. However, little is known on signals coordinating organ development and shape. Here we describe the characterization of a melon mutation *rf1*, leading to round fruit. Histological analysis of *rf1* flower and fruits revealed fruit shape is determined at flower stage 8, after sex determination and before flower fertilization. Using positional cloning, we identified the causal gene as the monoecy sex determination gene *CmACS7*, and survey of melon germplasms showed strong association between fruit shape and sexual types. We show that CmACS7-mediated ethylene production in carpel primordia enhances cell expansion and represses cell division, leading to elongated fruit. Cell size is known to rise as a result of endoreduplication. At stage 8 and anthesis, we found no variation in ploidy levels between female and hermaphrodite flowers, ruling out endoreduplication as a factor in fruit shape determination. To pinpoint the gene networks controlling elongated versus round fruit phenotype, we analyzed the transcriptomes of laser-capture microdissected carpels of wildtype and *rf1* mutant. This high resolution spatio-temporal gene expression dynamics revealed the implication of two regulatory modules. The first module implicates *E2F-DP* transcription factors, controlling cell elongation versus cell division. The second module implicates OVATE and TRM5-related proteins, controlling cell division patterns. Our finding highlights the dual role of ethylene in the inhibition of the stamina development and the elongation of ovary and fruit in cucurbits.

Introduction

Fruit, the mature ovary of a flower, is a vital structure in the sexual life cycle of angiosperms. Fruit development is initiated by ovule fertilization which promotes the ovary wall to undergo development and differentiation into fleshy or dry fruits. At maturity, fruits enclose and protect seeds, and aid in their dispersal. In angiosperms, fruit initiation and development share evolutionary conserved biological processes but at maturity exhibit an extraordinary diversity in terms of color, size and shape. This diversity is driven by Darwinian natural selection and thousands of years of artificial selection of fruit traits relevant to fruit production and marketing. For instance, fruit attributes such as size and shape are important in fruit harvesting and packaging, with consequences on transportation. Fruit appearance has also a major influence on consumers, preferring fruits of equal weight and uniform shape[1].

Fruit shape is the result of coordinated spatio-temporal regulation of cell division and expansion. The genetic basis of fruit shape has been assigned to a limited number of genes in several crops[2-8]. In tomato, a model species of fruit shape, five genes have been shown to control fruit shape and development, *FASCIATED (FAS), LOCULE NUMBER (LC), SUN, OVATE, Ovate-family protein* (*SlOFP20*) and *TONNEAU1 RECRUITING MOTIF 5* (*SlTRM5*)[9-14]. *LC* and *FAS*, orthologs of *WUSCHEL* and *CLAVATA3* transcription factor, respectively, influence the tomato fruit shape through the regulation of the number of fruit locules[9,11,15]. *SUN*, a member of the IQ67 Domain (IQD) protein family positively regulates fruit elongation[12,16,17]. *OVATE*, the founding member of the OVATE-family proteins (OFPs), encodes a protein with a conserved ~70 amino acid C-terminal domain, the OVATE/DUF623 domain[18]. Wild type *OVATE* and *SlOFP20* regulate fruit shape through repression of cell division in the longitudinal axis and enhance cell division along

the transversal axis[10,14,19]. SlTRM5, a member of the Arabidopsis TRM1-5 clade, interacts with OVATE to regulate cell division in developing ovaries[14].

The *Cucurbitaceae* is one of the angiosperm families with the most diverse fruits. For instance, fruit size of wild melon (*Cucumis melo* var. *agrestis*) and cucumber (*Cucumis sativus* var. *hardwickii*) are quite small, weighing less than 50 grams[20]. By contrast, *Atlantic Giant* variety of pumpkin (*Cucurbita maxima*) hold the world record of fruit weight, reaching 1056 kilograms[21]. Fruit shape is also very diverse. Fruits of the *flexuosus* melon varieties can reach more than two meters length with a fruit growth rate of nine centimeters per day[22]. Fruit shape is also very diverse in bottle gourd and squash (*Cucurbits pepo*) with spherical, cylindrical, elongated, curved, oblate, obovoid, drum-shaped, pear-shaped, spindle-shaped or crooked neck forms[23,24]. Owing to this extraordinary diversity of fruit shapes and sizes, *Cucurbitaceae* are excellent model systems to understand the molecular mechanisms governing fruit development.

Several studies have reported major QTLs controlling cucurbit fruit shapes[1,2,25-27]. In cucumber, *CsFUL1*, *Short fruit 1* (SF1) and *SF2* encode a FRUITFULL-like MADS-box transcription factor, a cucurbit-specific RING-type E3 ligase and a histone deacetylase complex 1 homologue, respectively[28-30]. *CsFUL1* represses the expression of *CsSUPERMAN* and inhibits auxin transport and thereby regulates cell division and expansion[30]. In melon, the fruit shape QTL *fsqs8.1/CmFSI8* encodes an OVATE family protein, CmOFP13, orthologous to SlOFP20[31,32].

Interestingly, some of the cucurbit fruit shape QTLs were shown to be associated with sex determination genes[2,3,33]. In melon, the fruit shape QTL *fs2.2* co-segregates with the *Monoecy* (separate male and female flowers on the same plant) gene, *CmACS7,* encoding for 1-aminocyclopropane-1-carboxylic acid synthase*,* the rate-limiting enzyme in ethylene

biosynthesis[1,2,34]. Similarly, in cucumber, the QTL controlling the transition between elongated and round fruit co-segregates with *CmACS7* orthologous gene, *CsACS2*[3,33,35]. Ethylene is also a key hormone in higher plants commonly associated with fruit ripening[36,37]. Although genetic associations between *Cucurbitaceae* sex determination genes and fruit development have been proposed, little is known about the link between sex determination, ethylene production and cellular and molecular mechanisms involved in *Cucurbitaceae* fruit shape determination.

Here, we report the cloning and characterization of a new melon mutant, *round fruit 1* (*rf1*), which encodes a null allele of *CmACS7*. We reveal how ethylene produced by *CmACS7* controls cell division and elongation, providing mechanistic insights into fruit shape regulation in plants.

Results

Elongated versus round fruit shapes are determined before flower anthesis

The melon inbred line Charentais Mono is a monoecious breeding line producing elongated fruit. To identify genes controlling fruit shape, we produced an ethyl methanesulfonate (EMS) mutagenized collection from Charentais Mono line. Phenotyping of 10 000 M2 plants corresponding to 1 000 M2 families led to identification of one mutant with rounded fruits (*rf1,* Figures 1A and 1B). To measure the roundness of *rf1* fruits we calculated the fruit shape index (FSi) as the ratio of the fruit length by the fruit diameter at mature stage. We found fruit length significantly longer in Charentais Mono line (WT) compared to *rf1* mutant. In contrast, fruit diameter did not significantly differ (Figures 1C and 1D), leading to FSi of 1.59 for the WT and 1.34 for the *rf1* mutant (Figure 1E). To pinpoint when melon fruit shape is determined, we

105 measured FSi of developing fruits of WT and *rf1* plants, starting from fertilized flower at anthesis
106 stage to mature fruit (Figure S1). We found significant differences of FSi between WT and *rf1*
107 plants, at all investigated fruit developmental stages, suggesting that melon fruit shape is
108 determined before flower fertilization (Figures S1A-S1C). To validate this we measured the
109 ovary shape index (OSi) as the ratio of the ovary length by the ovary width at anthesis stage and
110 before flower fertilization. As for the fruits, we found ovary length significantly longer in WT
111 compared to *rf1* mutant and no significant difference in the width of the ovaries (Figures 1F-1J),
112 leading to OSi of 2.58 for the WT and 1.95 for the *rf1* mutant (Figure 1J). Based on this we
113 concluded that elongated versus round fruit shape is determined during ovary development and
114 before flower fertilization.
115 To investigate the inheritance of the round fruit phenotype, *rf1* plants were back crossed to WT.
116 Consistent with *rf1* being a recessive mutation, F1 hybrid plants developed elongated fruits with
117 FSi similar to WT plants (Figures 1C-1E). Analysis of the F2 population showed 3:1 segregation
118 of elongated versus round fruit phenotypes, consistent with the hypothesis *rf1* is a single-locus
119 recessive mutation leading to round fruit (Table S1).
120
121 **_rf1_ locus encodes 1-aminocyclopropane-1-carboxylic acid synthase**
122 To identify *rf1* causal mutation, we sequenced bulked-genomic DNA from M2 plants producing
123 elongated fruits versus round fruits and determined the delta-SNP index. Four SNPs with Δ(SNP
124 index) superior to 0.5 and mapping to chromosome 2 telomeric region were found linked to *rf1*
125 (Figure 1K). Fine mapping further delimited *rf1* to G1504A transition leading to D279N
126 missense mutation in the sex determination gene *CmACS7* (Figures 1L and 1M). Primary and
127 tertiary protein structure analysis revealed D279N amino acid modification altering a highly

128 conserved protein domain, implicated in the binding of the enzyme cofactor, the pyridoxal 5'-
129 phosphate (PLP)[38,39] (Figures 1N and S2A-S2B). To investigate whether D279N mutation affects
130 CmACS7 enzymatic activity, we expressed His-tagged recombinant CmACS7 and CmACS7^{D279N}
131 proteins and assayed their activity *in vitro* by monitoring 5′-methylthioadenosine (MTA)
132 formation at different PLP concentrations. The enzymatic assays showed that CmACS7^{D279N}
133 displays very low ACS activity at all PLP concentrations (Figure 1O). These results indicate that
134 CmACS7-mediated ethylene production likely leads to the development of elongated fruits,
135 whereas loss of enzymatic activity leads to round fruits.
136 Previously, we showed that *CmACS7* plays a major role in sex determination and that loss of
137 CmACS7 enzymatic activity leads to the female to hermaphrodite sexual transition[40]. Consistent
138 with this, we found *rf1* plants andromonoecious, developing male and hermaphrodite flowers
139 (Figure S1). To test further the correlation between the development of female flowers and
140 elongated fruit, we phenotyped our previously reported *CmACS7* mutants, *CmACS7^{G19E}*,
141 *CmACS7^{A57V}* and *CmACS7^{D376N}*, for fruit shape. CmACS7^{G19E} and CmACS7^{A57V} isoforms
142 showed reduced ACS enzymatic activity whereas CmACS7^{D376N} isoform is mutated in a
143 nonconserved amino acid position predicted to not impair the protein function[40] (Figure S2C).
144 We found all the mutations leading to female to hermaphrodite flower sexual transition also lead
145 to round fruit development (Figures S1D-S1S). Conversely, the mutation *CmACS7^{D376N}*, not
146 altering sex of the flower do not alter fruit shape.
147 To test if this correlation occurs also in cucumber, we phenotyped five *CsACS2* mutants for fruit
148 development[41]. CsACS2^{G33C}, CsACS2^{P209S} and CsACS2^{S399L} isoforms showed reduced to no
149 ACS enzymatic activity whereas CsACS2^{S238F} and CsACS2^{S249F} isoforms are impaired in
150 nonconserved amino acid positions predicted to not impact the protein function[41]. As in melon,

CsACS2 loss of function mutants, *CsACS2*^{G33C}, *CsACS2*^{P209S} and *CsACS2*^{S399L}, developed hermaphrodite flowers and round fruits, whereas mutants not impaired in ACS activity, *CsACS2*^{S238F} and *CsACS2*^{S249F}, developed female flowers and elongated fruits (Figure S3). As the loss of the enzymatic activity of CmACS7/CsACS2 is associated with round fruit development, ethylene is likely a positive activator of elongated fruit growth. To test this hypothesis, we treated monoecious melon plants with 400 ppm of the ethylene perception inhibitor, silver nitrate, and phenotyped the developed fruits for fruit shape. As expected, treated plants developed hermaphrodite flowers and round fruit (Figure S1T). In summary, these data strongly validate the role of the ethylene produced in the flower by the monoecy genes in the development of elongated fruits.

CmACS7 loss of function allele is associated with round fruit melon accessions.

Previously, we have shown that *CmACS7* has a strong selective sweep signal and has experienced a recent positive selection in andromonecious accessions[40]. To explore the association between *CmACS7*^{A57V} loss of function allele[40] and fruit shape, we characterized fruit shape in a panel of 190 *Cucumis melo* melon accessions encompassing 15 horticultural groups and 2 sexual types, monoecious and andromonoecious (Figures 2A-2V and Table S2). At least three fruit per accession were measured and the average FSi was calculated. Classification according to *CmACS7* or *CmACS7*^{A57V} genotype showed that accessions carrying functional *CmACS7* allele develop fruit significantly longer than accessions carrying *CmACS7*^{A57V} loss-of-function allele (Figure 2W). This result was consistent with the comparison of female and hermaphrodite flowers in melon and cucumber (Figures S1 and S3) and confirmed the role of functional *CmACS7* in elongated fruit development.

We next examined the association of *CmACS7* and *CmACS7*^{A57V} alleles relative to fruit shape index (Figures 2X and 2Y). As observed for the entire panel (Figure 2W), *CmACS7*^{A57V} was strongly enriched in accessions developing round fruit (FSi < 1.5) particularly in the *cantalupensis*, *makuwa* and *reticulatus* horticultural groups (Figure 2Y and Table S2). In contrast, most of the elongated fruit accessions carry the WT *CmACS7* allele and *CmACS7*^{A57V} allele is almost absent in the *flexuosus* horticultural group (Figure 2X and Table S2). In view of the phenotypic association between fruit shape and flower sexual type, and the observed patterns and effects of allelic change in *CmACS7*, we concluded that the presence of round fruit shape in cultivated melon accessions is the consequence of the selection of the andromonoecious phenotype.

Elongated versus round fruit shapes is determined at stage 8 after flower sex determination

Characterization of *CmACS7/CsACS2* sex transition mutants for fruit shape strongly indicates *Monoecy* gene is pleotropic, controlling stamen inhibition in female flowers and the development of elongated fruit. To assess whether fruit shape is determined before, during or after sex determination we measured OSi of female and hermaphrodite flower buds at different developing stages (Figure 3). In melon, like in cucumber, female and hermaphrodite flowers at stage 4 are bisexual, developing both stamen and carpel primordia. At stage 6, stamen primordia stop developing in female flowers, leading, at stage 7, to sexually dimorphic female and hermaphrodite flowers[42]. We found no difference in OSi between female and hermaphrodite flower buds until stage 7 (Figures 3A-3E and 3H). At stage 8, we found ovary length significantly longer in WT compared to *rf1* mutant and no significant difference in the width of the ovaries (Figures 3F-3I). Based on this, we concluded that elongated versus round fruit shape

198 is determined during ovary development after sex determination. Consistent with this, *CmACS7*
199 is expressed in carpel primordia of flower buds at stage 4, when female and hermaphrodite buds
200 are not morphologically distinguishable[40]. Quantitative RT-PCR and *in-situ* hybridization show
201 that *CmACS7* is expressed at stage 8 and the accumulation of *CmACS7* mRNA is localized in the
202 central cells of the ovary (Figures 4B and 4C). Further, *CmACS7* expression level and pattern
203 were not different between female and hermaphrodite flowers (Figure 4C), a finding consistent
204 with the fact that *rf1* fruit shape is attributed to the loss of CmACS7 activity (Figure 1).
205
206 **Developmental and cellular changes leading to fruit shape determination**
207 Organ growth and shape are driven by both cell division and cell growth. These two processes are
208 coordinated but can be independently regulated. To quantify the contribution of the cellular
209 mechanism by which *CmACS7* controls fruit shape, we measured cell numbers and cell sizes
210 along longitudinal and transversal axis of WT female and *rf1* hermaphrodite flowers at stage 8
211 and at anthesis (Figures 4A, 4L and 4M). Although female and hermaphrodite flowers differed
212 significantly in ovary length, they do not differ with regard to cell number in the longitudinal axis
213 (Figure 4A). However, cell length was significantly longer in the WT female flowers. In the
214 transversal axis, we observed significantly more cells with smaller length and width in the *rf1*
215 hermaphrodite flowers. These results suggest that *CmACS7* may regulate fruit length by
216 mediating cell expansion and repressing cell division (Figure 4A).
217 To investigate whether the cell expansion differs uniformly throughout the ovary length,
218 individual cell file along longitudinal axis of female and hermaphrodites flowers was divided into
219 consecutive sectors of 10 cells and measured (Figure 4E). We observed that the average cell
220 length was similar in the top (cells 1 to 30) and bottom ovary ends (cells 110 onwards) (Figures

4D, 4F, 4G, 4J and 4K) whereas cells in the sector encompassing the 31st to 110th cells, expressing *CmACS7*, were significantly longer in female compared to hermaphrodite flowers (Figures 4D, 4H and 4I).

Endoreduplication is known to be associated with the increase in organ/cell size including fruits[43,44-46]. To test whether the cell size increase in WT compared to *rf1* is due to endoreduplication, we measured the ploidy level of ovary cells of female and hermaphrodite flowers at stage 8 and at anthesis. We observed for both WT and *rf1* flowers similar ploidy levels, indicating that endoreduplication may not contribute to the observed shape difference (Figures 4N and 4O).

Overall, the results demonstrate that CmACS7-mediated ethylene biosynthesis positively regulates cell elongation, leading to ovary and thus fruit elongation.

Ethylene modulates the expression of cell division and cell elongation promoting genes

At early fruit developmental stages, *CmACS7* mRNA accumulates in the central cells of the ovary (Figure 4B). To obtain an in-depth resolution of the molecular mechanisms controlling ovary shapes, we examined the transcriptome of laser capture microdissected (LCM-seq) ovary cells from the central part of female and hermaphrodite flower buds at stages 4 and 8 (Figures 5A-5C). Pairwise comparisons showed that female flowers at stage 8 (G8) are the main contributor of differentially expressed genes (Figures 5D, S4A and S4B). Overall, we found 2803 upregulated and 2363 downregulated genes in G8 (Data S1).

Consistent with the loss of CmACS7 function explaining the phenotypic variation, we observed many genes involved in ethylene pathway upregulated in G8 (Figure S4E). We grouped the differentially expressed genes by their expression patterns into two clusters, reflecting up- or

downregulated genes in the G8 samples (Figures 5E, S4C and S4D). Gene Ontology (GO) term enrichment analysis revealed cluster 1 enriched in GO terms related to response to stimulus, chemical or hormone and cell communication (Figure 5F). In contrast, cluster 2 was enriched in GO terms related to cell division and expansion including translation, DNA metabolic process, cell cycle, cellular process and microtubule-based movement (Figure 5G). Given the role of cell division and expansion in melon fruit shape, we examined the differentially expressed genes and observed that more than two-third of the genes related to cell division (GO:0051301) were downregulated in G8 compared to G4, H4 and H8 samples (Figure S5A), corroborating the reduced number of cells across the ovary width in G8 compared to H8 buds (Figure 4). In contrast, many members of the xyloglucosylate endotransglucosylase/hydrolase (XTH) family, known to govern cell enlargement, were upregulated in G8 compared to H8 buds (Figure S5B). RT-qPCR analysis confirmed the upregulation of *XTH* genes in G8 (Figures 5H-5K).

Functional annotation further identified several transcription factors (TFs) of the *E2F-DP* family downregulated in G8 compared to H8 (Figures S5D and S5E). *E2F-DPs* are TFs known to control cell cycle transition in both plants and animals[47-49]. In *Arabidopsis*, overexpression of *E2F* has been shown to suppress cell elongation and promotes cell division in cotyledons and hypocotyls[47,50]. Besides, *SWI/SNF-BAF60* TFs, known to inhibit cell elongation in *Arabidopsis* hypocotyl[51], were also found downregulated in G8 compared to H8 (Figure S5E).

OVATE family proteins (OFPs) have been shown to regulate plant organ size. In tomato, rice and peach, overexpression of *OFP* genes leads to small rounder fruits[8,10,19]. To regulate cell division and expansion patterns, OFPs interact with Tonneau1 Recruitment Motif (TRMs) proteins[14]. To assess the role of *OFPs* and *TRMs* in melon fruit shape, we have identified 21 OFPs and 39

TRMs melon proteins orthologous to Arabidopsis and tomato OFPs and TRMs proteins (Figures S6A and S6B). Current transcriptomic analysis and RT-qPCR revealed that among the differentially expressed genes, *OFPs* gene expression was mainly downregulated in G8 compared to H8 samples (Figures 5L-5O). In contrast, *TRMs* were mainly upregulated in G8 compared to H8 (Figures 5P-5R).

Discussion

The plant hormone ethylene plays a key role in development, senescence and adaptation to biotic and abiotic stresses[52,53]. In cucurbits, flower and fruit development can be divided into five major phases: the initiation of floral organs, the sexual dimorphism, the flower anthesis, the fruit development and the fruit maturation. Ethylene intervenes as positive and negative regulator through all these developmental phases[54]. Specifically for the flower developmental phase, we previously showed that ethylene is the key hormonal switch controlling sexual organs development[40,41,55,56]. Here we demonstrate that ethylene controls fruit shape after the sex determination and before the flower anthesis phase.

Organ shapes (e.g. fruit shape) is the result of coordinated spatial-temporal cell division and expansion. We show that CmACS7/CsACS2-mediated ethylene production is necessary for both the development of elongated fruits and female flower development (Figures 1, S1 and S3), consistent with the mapping of the fruit shape QTL *FS2.2* at vicinity of the *Monoecy* locus controlling sex determination in melon[2].

289 In melon, genetic diversity analysis has shown that *CmACS7* allele leading to andromonoecy is
290 under recent positive selection[40] to either permit flexibility in resource allocation to male and
291 female function[57-60], or for elevating male function, to increase pollen donation[61]. Besides flower
292 sex determination, fruit shape is another important domestication trait in vegetable and fruit
293 crops. To analyze the relation between fruit shape and sex determination, we investigated 190
294 melon accessions that display diverse fruit shapes and sexual types (Figure 2). We found that
295 monoecious accessions develop fruits longer than those of andromonoecious accessions (Figure
296 2W). Previously, we have demonstrated that *CmACS7*^{A57V} allele is monophyletic and under recent
297 positive selection in andromonoecious melon accessions[40]. Here, we also show that *CmACS7*^{A57V}
298 allele prevails in melon accessions developing round fruits (Figure 2Y). These data further
299 demonstrate that *CmACS7*-mediated fruit shape and sexual determination has been co-selected
300 during melon domestication and further spread by continuous selection of new varieties
301 worldwide. It is important to highlight that even though most melon accessions harboring the
302 *CmACS7*^{A57V} allele develop round fruits, we found some accessions with the *CmACS7*^{A57V} allele
303 developing elongated fruits (Figure 2X). To correct the round shape melon breeders have
304 screened melon germplasms and identified QTLs that modify fruit shape[1,27,62]. Recently, the
305 melon fruit shape QTL *fsqs8.1/CmFSI8* was shown to encodes the OVATE family protein
306 CmOFP13, orthologous to AtOFP1 and SlOFP20[31,32]. Variations at the *CmOFP13* locus could
307 explain the round fruit phenotype observed in melon accessions harboring the *CmACS7* allele
308 (Figure 2Y).
309
310 *CmACS7/CsACS2* expression inhibits stamen development in a non-cell-autonomous way[40,41]. In
311 contrast, *in situ* expression analysis showed *CmACS7* expression coincides with the cell

312 enlargement zone in the central region of developing ovaries, pointing toward cell-autonomous
313 control of fruit shape (Figure 4). LCM-seq analysis identified two clusters of gene expression
314 patterns, corresponding to genes up or down regulated in G8, respectively. Consistent with the
315 histological analysis pointing toward inhibition of cell division and enhanced cell elongation as
316 the cause of elongated fruit shape, we found down regulation of *E2F-DPs* and *SWI/SNF-BAF60*
317 TFs known to suppress cell elongation and promote cell division[47,50,51].
318 Regulation of microtubule orientation is an important step in cellular regulation of organ shape[63-
319 66]. We found *OFPs* genes downregulated and *TRMs* genes upregulated in female compared to
320 hermaphrodite flower buds (Figure 5). TRMs proteins interact with TONNEAU1 (TON1) and
321 Protein Phosphatase2A (PP2A) to target the TTP (TON1–TRM–PP2A) complex to cortical
322 microtubules to delineate the location of the cell division plane[67-69]. The contrasting expression of
323 *OFPs* and *TRMs* genes corroborate with the cell size and number differences observed in the fruit
324 shape controlling zone of the ovary. Consistent with this, overexpression of *OFPs* or loss-of-
325 function mutations in *TRMs* resulted in rounder fruits[8,14,19,67] and QTLs controlling fruit shape
326 were found mapping at the vicinity of *OFPs* or *TRMs* genes[14,70,71]. In Arabidopsis,
327 overexpression of *AtTRM1* and *AtTRM2* resulted in elongated organs[72]. GO enrichment analysis
328 also revealed major changes in genes related to microtubule-based movement (Figure 5G). The
329 process of cell division and expansion requires dynamic spatial reorganization of microtubule
330 network. Kinesins are a superfamily of microtubule-dependent motor proteins and they play
331 critical roles in various processes such as cell division and alteration of cell morphology[73].
332 Surprisingly, transcripts for majority of the differentially expressed kinesin proteins were found
333 to be downregulated in G8 compared to H8 (Figure S5C). It would be interesting to study the role
334 of kinesins in governing the fruit length, if any. XTH enzymes are a large family of cell wall-

modifying enzymes that play a central role in the cell wall expansion and re-modelling. We found a large number of XTH enzymes upregulated in cells undergoing enlargement. These protein family were also found to be induced by ethylene in rose, arrowhead tubers and persimmon[74-76], pointing toward a general mechanism controlling expression of XTH enzymes by ethylene.

Treatment of melon plant with ethylene perception inhibitor, silver nitrate led to transition from elongated to round ovary and fruit development. In *Ranunculus sceleratus*, ethylene treatment has been shown to promote petiole elongation growth[77]. These two experiments highlight the dual role of ethylene as an inhibitory-hormone for cell division rate and a promoting-hormone for cell enlargement. Recently, fine-tuning of ethylene homeostasis through a RING-type E3 ligase was also reported to control cucumber fruit elongation, suggesting conserved mechanisms controlling organ shape in plants[28].

In summary we propose a model in which *CmACS7* orchestrate sex determination and flower and fruit shape. Expression of *CmACS7* inhibits stamen development in non-cell-autonomous manner and promotes cell elongation in the carpel to lead to elongated fruit, in a cell-autonomous manner. This process includes activation of cell elongation and inhibition of cell division mechanisms. At the molecular level ethylene produced locally by CmACS7 lead to repression of cell division promoting genes and upregulation of cell elongation promoting genes. These processes occur after the flower acquire their sexual identity and before flower anthesis (Figure 6).

Acknowledgments

The authors thank Pascal Audigier, Florie Vion and Holger Ornstrup for taking care of the plant and the research facilities provided by the Institute of Plant-Science Paris-Saclay (IPS2, France). We thank the Center of Biological Resources CRBLeg of GAFL Avignon for maintaining, characterizing and providing melon genetic resources and the experimental unit, UE AHM of Avignon for their technical expertise. We thank Mickael Bourge (Flow cytometry platform I2BC) and Cecile Raynaud (IPS2) for their help with the flow cytometry analysis. Financial support was provided by the European Research Council (ERC-SEXYPARTH, 341076), the ANR EPISEX Project (ANR-17-CE20-0019), LabEx Saclay Plant Sciences (SPS) (ANR-10-LABX-40-SPS), and the Plant Biology and Breeding Department of INRAE.

Author contributions

C.T. and S.F. contributed to the generation of the mutant lines; C.C. contributed to the laser capture microdissection; A.Bo., S.B. and R.D performed bioinformatic analyses and contributed to the gene expression analysis; S.B. and H.M. performed the cell biology and histological experiments; N.G., C.D., S.F. A.Bo. carried out the plant phenotyping of melon lines and accessions; A.Bo., C.D. and A.Be. conceived and designed the study, supervised the work, analyzed the data and wrote the manuscript.

Declaration of Interests

The authors declare no competing interests.

Figure legends

Figure 1. *rf1* develops round fruit and encodes *CmACS7*.

(**A,B**) Elongated (**A**) and round (**B**) fruit developed on WT and *rf1* mutant plant, respectively. Bars= 5 cm. (**C-E**) Boxplots of fruit length (**C**), fruit diameter (**D**) and fruit shape index (**E**) in the WT, *rf1* and F1 plants (n=10). (**F,G**) Flowers of WT (**F**) and *rf1* (**G**) plants at anthesis. Bars= 1 cm. (**H-J**) Boxplots of ovary length (**H**), ovary width (**I**) and ovary shape index (**J**) in the WT, *rf1* and F1 plants (n=20). Data in (**C-E**) and (**H-J**) are displayed as box plot whiskers representing ±1.5× the interquartile range; horizontal lines, medians. ***, $P < 0.001$ (two-tailed Student's *t*-test). (**K-M**) Cloning of the rf1 locus. (**K**) The delta SNP indx (ΔSNP index) between elongated and round bulks. (**L**) Schematic of the mapping region of the rf1 locus. The green and blue arrows represent annotated genes. Orange dashed lines indicate the physical position of the induced EMS mutations. (**M**) Structure of the *CmACS7* gene and position of the missense induced mutation D279N. Green boxes and black lines represent exons and introns, respectively. (**N**) Amino acid alignments of CmACS7 with homologous proteins from *Cucumis sativus (Cs*), *Vitis vinifera* (*Vv*), *Cucurbita maxima* (*Cmax*), *Arabidopsis thaliana* (*At*), *Solanum lycopersicum* (*Sl*), *Petunia hybrida* (*Ph*), *Medicago truncatula* (*Mt*), *Momordica charentia* (*Mc*), *Triticum aestivum* (*Ta*) and *Picea glauca* (*Pg*). Numbers above the alignment indicate the amino acid positions along the CmACS7 protein. Box 5 indicates a conserved domain in ACS proteins. (**O**) Effect of PLP concentration on the ACS enzymatic activity of CmACS7 (blue bars) and D279N (orange bars) protein forms. See also Figures S1-S3 and Table S1.

Figure 2: Round fruit phenotype is associated with *CmACS7*^{A57V} allele.

(**A-V**) Morphological variation of melon fruits from the diversity panel (n=190) representing 15 horticultural groups. (**A,B**) *acidulus,* (**C**) *agrestis,* (**D**) *ameri,* (**E**) *chandalak,* (**F**) *chate,* (**G**) *chinensis,* (**H**) *chito,* (**I**) *dudaim,* (**J,K**) *flexuosus,* (**L-N**) *inodorus,* (**O**) *cantalupensis,* (**P**) *conomon,* (**Q-T**) *makuwa,* (**U**) *momordica,* (**V**) *reticulatus.* The picture shows a compilation of fruits from the diversity panel with different colors, shapes, and sizes to illustrate the phenotypic variation present of the fruit shape in melon. For more details please see Table S2. Bar=10 cm. (**W**) Boxplots of fruit shape index. Data are displayed as box plot whiskers representing ±1.5× the interquartile range; horizontal lines, medians. *p*=5.1e-4 (two-tailed Student's *t*-test). (**X,Y**) Allele frequencies of *CmACS7* and *CmACS7*^{A57V} in melon accessions developing elongated fruits (n=74) (**X**) and round fruits (n=116) (**Y**). See also Table S2.

Figure 3: Fruit shape is determined after sex determination,

(**A,B**) Confocal images of WT (**A**) and *rf1* (**B**) flowers at stage 5 before sexual dimorphism. St, stamen; C, carpel. Bars= 100 µm. (**C-E**) Carpel length (**C),** carpel cell number (**D**) and average cell length (**E**) in the longitudinal axis of WT and *rf1* flowers at stage 5. Values are means ±s.d. derived from 3 flowers. (**F,G**) Confocal images of WT (**F**) and *rf1* (**G**) flowers at stage 8 after sexual determination. Bars= 500 µm. (**H-I**) Ovary length (**H**) and width (**I**) of WT and *rf1* flowers at different developmental stages (n=9). Data in (**H**) and (**I**) are displayed as box plot

whiskers representing ±1.5× the interquartile range; horizontal lines, medians. ***, $P < 0.001$ (two-tailed Student's *t*-test).

Figure 4: Cell number and cell length of ovaries from WT and *rf1* flowers.

(**A**) Characteristics of ovaries from WT and *rf1* flowers. Values are means ±s.d. derived from 7 flowers.. (**B**) *CmACS7 in situ* expression at flower developmental stage 8. Bar= 250 µm. (**C**) Quantitative real-time PCR of *CmACS7* in WT and *rf1* flowers at stage 8. Values are means ±s.d. of three biological replicates. (**D**) Cell length averaged from consecutive sectors of 10 cells along the longitudinal axis of the ovary. Values are means ±s.d. derived from 5 flowers. (**E**) Longitudinal cell layers of WT melon flower at stage 8. Bar= 10 µm. (**F-K**) Magnification of the WT (**F,H,J**) and *rf1* (**G,I,K**) flower cross-section in the apical (**F,G**), median (**H,I**) and basal (**J,K**) ovary regions. Bars= 25 µm. (**L**) Boxplots of Cell length and (**M**) cell width at flower anthesis (n=10). Data in (**L,M**) are displayed as box plot whiskers representing ±1.5× the interquartile range; horizontal lines, medians. (**N,O**) Ploidy analysis by flow cytometry in WT and *rf1* flowers at stage 8 (**N**) and at anthesis (**O**). Values are means ±s.d. of five biological replicates. Statistical *p* values are calculated using two-tailed Student's *t*-test. n.s: no statistically significant difference. See also Table S3.

Figure 5: Gene expression profiling of female and hermaphrodite flowers by LCM-Seq.

(**A-C**) Laser capture microdissection of the ovary median region expressing *CmACS7*. (**D**) Differentially expressed genes in pairwise comparison groups. (**E-G**) Gene-wise hierarchical

clustering heat map (**E**) of all 5,166 differentially expressed genes (adjusted *P* value < 0.001) showing segregation into two clusters. The *z*-score scale represents mean-subtracted regularized log-transformed read counts. (**F**) Cluster 1 (*n* = 2,803) includes genes with increased expression in female flowers at stage 8 (G8). (**G**) Cluster 2 (*n* = 2,363) includes genes downregulated in G8. Data in (**F**) and (**G**) are displayed as box plot whiskers representing ±1.5× the interquartile range; horizontal lines, medians. Enriched GO terms are shown to the right. (**H-R**) Quantitative real-time PCR of cell expansion (**H-K**), *OFPs* (**L-O**) and *TRMs* (**H-J**) genes in female and hermaphrodite flowers. Values are means ±s.d. of three biological replicates. *, $P < 0.05$; **, $P < 0.01$ ***, $P < 0.001$ (two-tailed Student's *t*-test). H4, hermaphrodite flower at stage 4; G4: female flower at stage 4; H8, hermaphrodite flower at stage 8; G8: female flower at stage 8. See also Figures S4-S6, Table S3 and Data S1.

Figure 6. Proposed model for *CmACS7*-dependent regulation of melon fruit shape.

At developmental stage 5, female and hermaphrodite carpel-bearing flowers express functional or non-functional CmACS7 protein isoform in the carpel, respectively. Functional CmACS7 isoform produces ethylene repressing the development of stamens and leading to the development of female flowers. After sexual differentiation, at stage 8, *CmACS7* continues to be expressed and to produce ethylene in the developing carpels. Ethylene downregulates the expression of *OFPs*, *E2F-DPs* and *SWI/SNF-BAF60* genes and induces the expression of *TRMs* and *XTHs* genes leading to cell elongation and the development of elongated fruit. Expression of the nonfunctional $CmACS7^{D279N}$ isoform results in the expression of *OFPs*, *E2F-DPs* and

464 *SWI/SNF-BAF60* genes and downregulation of *TRMs* and *XTHs* genes leading to induced cell
465 division, reduced cell elongation and finally to the development of round fruit.

466

467

STAR Methods

RESOURCE AVAILABILITY

Lead contact

Further information and requests for resources and reagents should be directed to and will be fulfilled by the Lead Contact, Abdelhafid Bendahmane (abdelhafid.bendahmane@inrae.fr).

Materials availability

This study did not generate new unique reagents.

Data and code availability

Accession numbers are listed in the key resources table. This paper does not report original code. The high-throughput sequencing datasets generated in this study have been deposited in the Sequence Read Archive (SRA) under the accession number PRJNA814521. Other data supporting our findings are available in the manuscript file or from the corresponding author upon request.

EXPERIMENTAL MODEL AND SUBJECT DETAILS

Plant Material

The seeds of Charentais Mono line of melon (Cucumis melo L.) were treated with ethyl methanesulfonate (EMS) as described in Dahmani-Mardas et al.[78]. The M1 plants were self-pollinated, and the round fruit line *rf1* was identified in the M2 population. Then, *rf1* was crossed with the Charentais Mono line and an F2 population was derived from self-crossed F1 plants. Mutant melon lines harboring either of the $CmACS7^{D376N}$, $CmACS7^{G19E}$ and $CmACS7^{A57V}$ were used in this study[40]. Similarly, cucumber wild-type and mutant lines harboring either of the $CsACS2^{G33C}$, $CsACS2^{S238F}$, $CsACS2^{S249F}$, $CsACS2^{P209S}$ and $CsACS2^{S399L}$ were also used in this study[41,79]. Plants were grown in the greenhouse in the spring and summer under standard agronomic conditions and evaluated for flower sex type and fruit shape during three consecutive growing seasons. For the 190 melon accessions of the diversity panel, encompassing 15 horticultural groups and monoecious and andromonoecious sexual types, were grown at INRAE GAFL Avignon station. 2 plants for each accession were phenotyped and 3 fruits per plant were scored for mature fruit length, diameter and shape index. Representative fruits from each accession are shown in Figures 2A-2V.

METHOD DETAILS

Measurement of cell number and cell size

To measure the ovary cell size and number, fresh-picked flower buds from Charentais Mono and r*f1* plants were sampled at different developmental stages 4, 7, 8 and 9 and fixed in FAE solution (formaldehyde: acetic acid: 70% ethanol; 1:1:18 ration) for 24 hours and then washed four times

with 70% ethanol. For the measurements, flower buds were stained with 0.1 mM propidium iodide (Sigma-Aldrich) for 1 hour and longitudinal images were recorded using the Zeiss LSM 880 confocal microscope. The cell size and number were then calculated using Image J software. The means and standard errors were calculated from the measurements of at least 5 flower buds for each genotype. Student *t*-test was used to compare the cell number and cell size difference between the WT and *rf1* plants.

BSA-Seq Mapping Approach

To map the *rf1* causal mutation, an F2 population was constructed by crossing *rf1* mutant plant with WT Charentais Mono plant. More than 200 F2 plants were phenotyped and sampled for individual genomic DNA extraction. Mutant and WT pools were created by mixing equal ratio of genomic DNA from round-fruit and elongated-fruit F2 plants. Genomic DNA pools were shared for preparation of sequencing libraries following the recommendation of Illumina TruSeq DNA PCR-free prep kit. Reads of the two bulks (mutant and WT) were aligned to the reference melon genome[80]. For each bulk, the SNP-index across all loci was calculated as the proportion of reads that were different from the reference allele. The delta (Δ) SNP-index was calculated by subtracting the SNP-indices of the two bulks at each locus (SNP-index_mutant – SNP-index_WT).

Expression, purification and enzymatic activity assays of recombinant protein

Recombinant proteins, CmACS7 and CmACS7^{D279N}, were expressed, purified and assayed as described in Boualem et al.[40]. Briefly, *CmACS7* cDNAs from monoecious, and *CmACS7^{D279N}* TILLING mutant were cloned in pET-15b vector as His6-tagged proteins and expressed in *E. coli*

530 BL21(DE3)pLysS cells. Protein expression was induced by adding IPTG (0.5 mM) and cells
531 were grown for 5 hours at 25°C. Cells were harvested and disrupted on ice by sonication in the
532 lysis buffer using five pulses of 30 seconds at 20 kHz with 3 minutes cooling on ice between each
533 pulse. The supernatant separated from cell debris was applied to a Ni-IDA 15 ml column (Sigma,
534 France). Wild type (CmACS7) and mutant ($CmACS7^{D279N}$) forms of protein were then eluted
535 with the same buffer. CmACS7 and $CmACS7^{D279N}$ enzyme activity was determined by
536 monitoring the MTA formation. Specific activity measurement was performed on 3 different
537 enzyme preparations. Specific activities were measured on dialyzed enzymes in the presence of
538 60µM SAM and various PLP concentrations. Residual activities (%) corresponds to the specific
539 activity measured / specific activity measured for CmACS7 enzyme at 300µM PLP.

540

541

542 **Protein structure modeling**

543 The CmACS7 three-dimensional structures were generated using the Geno3D server
544 (http://geno3d-pbil.ibcp.fr). Superposition of the tomato ACS structure (1IAY.pdb) determined
545 by x-ray crystallography (81) and the CmACS7 model was carried out and visualized using the
546 Chimera server (http://www. cgl.ucsf.edu/chimera).

547

548 ***In situ* hybridization**

549 *CmACS7* in situ hybridization was performed as described in Boualem et al.[40]. Primers used for
550 this experiment are listed in Table S3.

551

552 **Identification of OFP and TRM proteins in melon.**

553 To identify candidate OFP and TRM proteins, the melon database
554 (http://www.cucurbitgenomics.org/) was searched first using the keywords 'OFP' or 'TRM'. In
555 addition, Arabidopsis and tomato OFP and TRM protein sequences were downloaded from The
556 Arabidopsis Information Resource (http://www.arabidopsis.org/) and the Sol Genomics Network
557 (http://solgenomics.net/), respectively. These sequences were used to identify homologous
558 peptides from melon by performing a BLASTP search at melon genome v3.5 database
559 (http://cucurbitgenomics.org/). The BLAST E-value was set to 1e−3. Finally, repeated and
560 incomplete sequences were removed manually and the non-redundant CmOFP and CmTRM
561 sequences were subjected to further analyses.

562

563 **Sequence and phylogeny analysis**

564 Multiple sequence alignment of full-length protein sequences of CmACS7 with homologous
565 proteins from *Cucumis sativus (Cs*), *Vitis vinifera* (*Vv*), *Cucurbita maxima* (*Cmax*), *Arabidopsis*
566 *thaliana* (*At*), *Solanum lycopersicum* (*Sl*), *Petunia hybrida* (*Ph*), *Medicago truncatula* (*Mt*),
567 *Momordica charentia* (*Mc*), *Triticum aestivum* (*Ta*) and *Picea glauca* (*Pg*) was performed using
568 the ClustalW (http://www.ebi.ac.uk/Tools/clustalw2). Phylogenetic trees were constructed by
569 MEGAX (http://www.megasoftware.net/index.html) based on the Neighbor-Joining method.

570

571 **Silver nitrate treatment**

572 To assess the effect of $AgNO_3$ on fruit shape, 400 ppm of the ethylene perception inhibitor,
573 $AgNO_3$ solution was periodically sprayed on the leaves of WT Charentais Mono line at 20
574 internodes developmental stage. About 3 weeks after treatment, perfect flowers appeared and

were selfed. The fruits developed from $AgNO_3$-induced hermaphrodite flowers were phenotyped for fruit shape index.

Flow Cytometry and ploidy analysis

To determine the flower ploidy level, young flower buds at stage 8 was chopped with a new razor blade in 1ml of nuclei-isolation buffer[82]. Suspended nuclei were filtered through a 40-µm Fisher brand cell strainer, treated with RNase (5U/mL), and stained with propidium iodide (0.001 µg/100 µL sample). Ploidy level of ~10.000 nuclei was determined using a Cyflow SL3 flow cytometer (Partec-Sysmex). Ploidy histograms were quantitatively analyzed with DPAC software (Partec).

Transcriptome sequencing from laser capture microdissected tissue

Transcriptomic analysis was carried out on laser capture microdissected central region of carpels for both female and hermaphrodite flowers from the WT Charentais Mono and *rf1* plants, respectively. Two different developmental stages (stages 4 and 8) were chosen such that the transcriptomic profiles can be compared before and after the divergence in ovary shape index (OSi) between the female and hermaphrodite flowers. Female and hermaphrodite flower buds at stage 4 were referred to as G4 and H4, respectively. Female and hermaphrodite flower buds at stage 8 were referred to as G8 and H8, respectively.

Tissue embedding

596 Flowers buds were fixed in RCL2 (Excilone) with 0.01% triton. For tissue fixation, samples were
597 placed under vacuum 4 times for 15 min and kept in the fixative overnight at 4 °C. Samples were
598 then dehydrated at 4 °C in a graded series of ethanol (70% for 30 min, 96% for 30 min, 100% for
599 3 × 30 min), followed by a graded series of ethanol:histoclear bath (3:1, 1:1, 1:3 for 1 h each).
600 Histoclear was then substituted by Surgipath Paraplast Plus tissue embedding media (Leica
601 Biosystems) and incubated overnight at 60 °C. Finally, flowers were embedded into paraffin
602 blocks, cooled and stored at −20 °C.

603 *Laser capture microdissection*

604 A Rotary microtome (HM 3555 Microtom) was used to cut 8 µm thick longitudinal sections of
605 the embedded flowers. Ribbon of flower sections were stretched on UV-treated, 1 mm PEN-
606 membrane covered slides (Arcturus Bioscience, Excilone) such that each slide corresponds to 15–
607 25 sections of flowers. Slides were deparaffinized, and laser capture microdissection was
608 immediately conducted on a Palm DIC FLUO Microdissection System (Zeiss). The contours of
609 central carpel sector encompassing the 31st to 110th cells were cut with the laser and target
610 regions were catapulted into Adhesive cap 500 clear (Zeiss).

611 *RNA extraction*

612 Immediately after dissection, cells were lysed using the PicoPure® RNA Isolation Kit (Arcturus
613 Bioscience, Excilone) and stored at −20 °C before RNA extraction. RNA quality and
614 concentration were evaluated with a Bioanalyser 2100 (Agilent Technologies) on Agilent RNA
615 Pico chips. RNA recovery ranged from 900–2000 pg/µl, with a RIN above 7.

616 *Preparation of the sequencing libraries*

617 2 ng of total RNA was used for each cDNA library preparation using the SMARTer Ultra Low
618 RNA Kit for Illumina Sequencing from Clontech according to manufacturer's instructions.

Libraries were sequenced on the HiSeq2000 platform Illumina® and 30 to 50 million paired-end reads per sample were obtained. Read quality was assessed using FastQC (version 0.11) and STAR (version 2.7) has been used to generate the mapping files. The mapped reads were assigned to genes with featureCount (v2.0.0). DESeq2 (version 1.30.1) was used to identify the differentially expressed (DE) genes (adjusted p value <0.001 and log2(FC)>1 or <-1).

Hierarchical clustering and GO analysis

The DE genes were subjected to hierarchical clustering analysis using Perseus to identify the co-expressed DE genes (83) GO enrichment analysis was performed on AgriGOv2 web server[84].

Reverse transcription polymerase chain reaction (RT-PCR) and qPCR

For the RT-qPCR, the total RNAs from laser capture microdissection experiments were used to validate the gene expression pattern. Primer design was performed with the Primer3 software (http://frodo.wi.mit.edu/cgi-bin/primer3/primer3_www.cgi). Primers sequences are listed in Table S3. To check specificity of the designed primers, all amplicons were sequenced and blasted against NCBI database. Polymerase chain reactions were performed in an optical 384-well plate with the Bio-Rad CFX96 Real-time PCR apparatus, with qPCR MasterMix Plus for SYBR® Green I w/o ROX (Eurogentec) and according to manufacturer's instructions. PCR amplification specificity was verified by a dissociation curve (55 °C to 95 °C). A negative control without cDNA, technical replicates on three independent synthesis of cDNA (derived from the same RNA sample), and three independent biological experiments were performed in all cases. Gene expression is normalized to the expression levels of housekeeping genes: *CmActin2* and *CmADP*

641 (primers shown in Table S3). The gene relative expressions were determined as described in
642 Eleblu et al.[85].
643
644 **Genotyping**
645 The genotyping of 81 melons accessions for the C to T nucleotide transition leading to A57V
646 amino acid substitution was carried out with the cleaved amplified polymorphic sequence
647 (CAPS) marker described in Boualem et al.[40] and on the basis of *Alu*1 restriction site
648 polymorphism. Briefly, melon genomic DNA was extracted from young leaves following CTAB
649 method and was used as matrix for *CmACS7* PCR amplification using primers described in Table
650 S3. PCR products were then digested by *Alu I* restriction enzyme to assess the presence absence
651 of the C to T nucleotide transition.
652
653 **QUANTIFICATION AND STATISTICAL ANALYSIS**
654 For the fruit and ovary shape phenotypic analysis in WT Charentais Mono and *rf1* plants, 10
655 fruits from at least 5 independent plants for each genotype were analyzed. For the ovary shape
656 phenotypic analysis, 20 flowers at anthesis from at least 5 independent plants for each genotype
657 were analyzed.
658 Statistical significance analysis between two groups was performed using the Student's *t*-test.
659 For RNA-seq analysis, pool of laser captured microdissected samples from 3 flower buds has
660 been used as one biological replicate. Three biological replicates were performed for RNA-seq.
661 For RT-qPCR analysis, the expression values correspond to the average of three biological
662 replicates, with three technical replicates.
663

664 # References

665 1. Diaz, A., Zarouri, B., Fergany, M., Eduardo, I., Alvarez, J.M., Pico, B., and Monforte,
666 A.J. (2014). Mapping and introgression of QTL involved in fruit shape transgressive
667 segregation into 'piel de sapo' melon (cucumis melo l.) [corrected]. PloS one *9*, e104188.
668 2. Perin, C., Hagen, L.S., Giovinazzo, N., Besombes, D., Dogimont, C., and Pitrat, M.
669 (2002). Genetic control of fruit shape acts prior to anthesis in melon (Cucumis melo L.).
670 Mol Genet Genomics *266*, 933-941.
671 3. Serquen, F.C., Bacher, J., and Staub, J.E. (1997). Mapping and QTL analysis of
672 horticultural traits in a narrow cross in cucumber (Cucumis sativus L) using random-
673 amplified polymorphic DNA markers. Mol Breeding *3*, 257-268.
674 4. Marguerit, E., Boury, C., Manicki, A., Donnart, M., Butterlin, G., Nemorin, A.,
675 Wiedemann-Merdinoglu, S., Merdinoglu, D., Ollat, N., and Decroocq, S. (2009). Genetic
676 dissection of sex determinism, inflorescence morphology and downy mildew resistance in
677 grapevine. Theor Appl Genet *118*, 1261-1278.
678 5. Doganlar, S., Frary, A., Daunay, M.C., Lester, R.N., and Tanksley, S.D. (2002).
679 Conservation of gene function in the Solanaceae as revealed by comparative mapping of
680 domestication traits in eggplant. Genetics *161*, 1713-1726.
681 6. Zygier, S., Chaim, A.B., Efrati, A., Kaluzky, G., Borovsky, Y., and Paran, I. (2005).
682 QTLs mapping for fruit size and shape in chromosomes 2 and 4 in pepper and a
683 comparison of the pepper QTL map with that of tomato. Theor Appl Genet *111*, 437-445.
684 7. Zhou, M.X., and Liu, T. (2020). Functional Analysis of Ovate Family Proteins (OFPs) in
685 Fruit Shape Formation in Strawberry (Fragaria ananassa). Hortscience *55*, S81-S81.

8. Zhou, H., Ma, R.J., Gao, L., Zhang, J.N., Zhang, A.D., Zhang, X.J., Ren, F., Zhang, W.H., Liao, L., Yang, Q.R., et al. (2021). A 1.7-Mb chromosomal inversion downstream of aPpOFP1gene is responsible for flat fruit shape in peach. Plant Biotechnol J *19*, 192-205.

9. Xu, C., Liberatore, K.L., MacAlister, C.A., Huang, Z., Chu, Y.H., Jiang, K., Brooks, C., Ogawa-Ohnishi, M., Xiong, G., Pauly, M., et al. (2015). A cascade of arabinosyltransferases controls shoot meristem size in tomato. Nat Genet *47*, 784-792.

10. Liu, J.P., Van Eck, J., Cong, B., and Tanksley, S.D. (2002). A new class of regulatory genes underlying the cause of pear-shaped tomato fruit. P Natl Acad Sci USA *99*, 13302-13306.

11. Munos, S., Ranc, N., Botton, E., Berard, A., Rolland, S., Duffe, P., Carretero, Y., Le Paslier, M.C., Delalande, C., Bouzayen, M., et al. (2011). Increase in Tomato Locule Number Is Controlled by Two Single-Nucleotide Polymorphisms Located Near WUSCHEL. Plant Physiol *156*, 2244-2254.

12. Xiao, H., Jiang, N., Schaffner, E., Stockinger, E.J., and van der Knaap, E. (2008). A retrotransposon-mediated gene duplication underlies morphological variation of tomato fruit. Science *319*, 1527-1530.

13. Snouffer, A., Kraus, C., and van der Knaap, E. (2020). The shape of things to come: ovate family proteins regulate plant organ shape. Curr Opin Plant Biol *53*, 98-105.

14. Wu, S., Zhang, B.Y., Keyhaninejad, N., Rodriguez, G.R., Kim, H.J., Chakrabarti, M., Illa-Berenguer, E., Taitano, N.K., Gonzalo, M.J., Diaz, A., et al. (2018). A common genetic mechanism underlies morphological diversity in fruits and other plant organs. Nat Commun *9,*4734.

709 15. van der Knaap, E., Chakrabarti, M., Chu, Y.H., Clevenger, J.P., Illa-Berenguer, E.,
710 Huang, Z.J., Keyhaninejad, N., Mu, Q., Sun, L., Wang, Y.P., et al. (2014). What lies
711 beyond the eye: the molecular mechanisms regulating tomato fruit weight and shape.
712 Front Plant Sci *5,* 227.
713 16. Wu, S., Xiao, H., Cabrera, A., Meulia, T., and van der Knaap, E. (2011). SUN Regulates
714 Vegetative and Reproductive Organ Shape by Changing Cell Division Patterns. Plant
715 Physiol *157*, 1175-1186.
716 17. Wu, S., Clevenger, J.P., Sun, L., Visa, S., Kamiya, Y., Jikumaru, Y., Blakeslee, J., and
717 van der Knaap, E. (2015). The control of tomato fruit elongation orchestrated by sun,
718 ovate and fs8.1 in a wild relative of tomato. Plant Sci *238*, 95-104.
719 18. Liu, D., Sun, W., Yuan, Y.W., Zhang, N., Hayward, A., Liu, Y.L., and Wang, Y. (2014).
720 Phylogenetic analyses provide the first insights into the evolution of OVATE family
721 proteins in land plants. Ann Bot-London *113*, 1219-1233.
722 19. Wang, S., Chang, Y., Guo, J., and Chen, J.G. (2007). Arabidopsis Ovate Family Protein 1
723 is a transcriptional repressor that suppresses cell elongation. Plant J *50*, 858-872.
724 20. Stepansky, A., Kovalski, I., and Perl-Treves, R. (1999). Intraspecific classification of
725 melons (Cucumis melo L.) in view of their phenotypic and molecular variation. Plant Syst
726 Evol *217*, 313-332.
727 21. Savage, J.A., Haines, D.F., and Holbrook, N.M. (2015). The making of giant pumpkins:
728 how selective breeding changed the phloem of Cucurbita maxima from source to sink.
729 Plant Cell Environ *38*, 1543-1554.
730 22. Ueda, J., Tanaka, K., and Kato, J. (1986). Plant-Growth Regulators in Cucumis-Melo L
731 Var Flexuosus Naud Fruit during Rapid Growth. Plant Cell Physiol *27*, 809-818.

732 23. Paris, H.S. (2016). Germplasm enhancement of Cucurbita pepo (pumpkin, squash, gourd:
733 Cucurbitaceae): progress and challenges. Euphytica *208*, 415-438.
734 24. Xu, P., Xu, S.Z., Wu, X.H., Tao, Y., Wang, B.G., Wang, S., Qin, D.H., Lu, Z.F., and Li,
735 G.J. (2014). Population genomic analyses from low-coverage RAD-Seq data: a case study
736 on the non-model cucurbit bottle gourd. Plant J *77*, 430-442.
737 25. Harel-Beja, R., Tzuri, G., Portnoy, V., Lotan-Pompan, M., Lev, S., Cohen, S., Dai, N.,
738 Yeselson, L., Meir, A., Libhaber, S.E., et al. (2010). A genetic map of melon highly
739 enriched with fruit quality QTLs and EST markers, including sugar and carotenoid
740 metabolism genes. Theor Appl Genet *121*, 511-533.
741 26. Monforte, A.J., Oliver, M., Gonzalo, M.J., Alvarez, J.M., Dolcet-Sanjuan, R., and Arus,
742 P. (2004). Identification of quantitative trait loci involved in fruit quality traits in melon
743 (Cucumis melo L.). Theor Appl Genet *108*, 750-758.
744 27. Monforte, A.J., Diaz, A., Cano-Delgado, A., and van der Knaap, E. (2014). The genetic
745 basis of fruit morphology in horticultural crops: lessons from tomato and melon. J Exp
746 Bot *65*, 4625-4637.
747 28. Xin, T., Zhang, Z., Li, S., Zhang, S., Li, Q., Zhang, Z.H., Huang, S., and Yang, X. (2019).
748 Genetic Regulation of Ethylene Dosage for Cucumber Fruit Elongation. Plant Cell *31*,
749 1063-1076.
750 29. Zhang, Z., Wang, B., Wang, S., Lin, T., Yang, L., Zhao, Z., Zhang, Z., Huang, S., and
751 Yang, X. (2020). Genome-wide Target Mapping Shows Histone Deacetylase Complex1
752 Regulates Cell Proliferation in Cucumber Fruit. Plant Physiol *182*, 167-184.
753 30. Zhao, J., Jiang, L., Che, G., Pan, Y., Li, Y., Hou, Y., Zhao, W., Zhong, Y., Ding, L., Yan,
754 S., et al. (2019). A Functional Allele of CsFUL1 Regulates Fruit Length through

Repressing CsSUP and Inhibiting Auxin Transport in Cucumber. Plant Cell *31*, 1289-1307.

31. Ma, J., Li, C., Zong, M., Qiu, Y., Liu, Y., Huang, Y., Xie, Y., Zhang, H., and Wang, J. (2022). CmFSI8/CmOFP13 encoding an OVATE family protein controls fruit shape in melon. J Exp Bot *73*, 1370-1384.

32. Martinez-Martinez, C., Gonzalo, M.J., Sipowicz, P., Campos, M., Martinez-Fernandez, I., Leida, C., Zouine, M., Alexiou, K.G., Garcia-Mas, J., Gomez, M.D., et al. (2021). A cryptic variation in a member of the Ovate Family Proteins is underlying the melon fruit shape QTL fsqs8.1. Theor Appl Genet *135*, 785-801.

33. Liu, S., Xu, L., Jia, Z., Xu, Y., Yang, Q., Fei, Z., Lu, X., Chen, H., and Huang, S. (2008). Genetic association of ETHYLENE-INSENSITIVE3-like sequence with the sex-determining M locus in cucumber (Cucumis sativus L.). Theor Appl Genet *117*, 927-933.

34. Rosa, J.T. (1928). The inheritance of flowers types in *Cucumis* and *Citrullus*. Hilgardia *3*, 233-250.

35. Pan, J., Wang, G., Wen, H.F., Du, H., Lian, H.L., He, H.L., Pan, J.S., and Cai, R. (2018). Differential Gene Expression Caused by the F and M Loci Provides Insight Into Ethylene-Mediated Female Flower Differentiation in Cucumber. Front Plant Sci *9*, 1091.

36. Wang, Y.H., and Irving, H.R. (2011). Developing a model of plant hormone interactions. Plant signaling & behavior *6*, 494-500.

37. Gapper, N.E., McQuinn, R.P., and Giovannoni, J.J. (2013). Molecular and genetic regulation of fruit ripening. Plant molecular biology *82*, 575-591.

776 38. Capitani, G., Hohenester, E., Feng, L., Storici, P., Kirsch, J.F., and Jansonius, J.N. (1999).
777 Structure of 1-aminocyclopropane-1-carboxylate synthase, a key enzyme in the
778 biosynthesis of the plant hormone ethylene. J Mol Biol *294*, 745-756.
779 39. Capitani, G., McCarthy, D.L., Gut, H., Grutter, M.G., and Kirsch, J.F. (2002). Apple 1-
780 aminocyclopropane-1-carboxylate synthase in complex with the inhibitor L-
781 aminoethoxyvinylglycine - Evidence for a ketimine intermediate. J Biol Chem *277*,
782 49735-49742.
783 40. Boualem, A., Fergany, M., Fernandez, R., Troadec, C., Martin, A., Morin, H., Sari, M.A.,
784 Collin, F., Flowers, J.M., Pitrat, M., et al. (2008). A conserved mutation in an ethylene
785 biosynthesis enzyme leads to andromonoecy in melons. Science *321*, 836-838.
786 41. Boualem, A., Troadec, C., Kovalski, I., Sari, M.A., Perl-Treves, R., and Bendahmane, A.
787 (2009). A Conserved Ethylene Biosynthesis Enzyme Leads to Andromonoecy in Two
788 Cucumis Species. PloS one *4,* e6144.
789 42. Bai, S.L., Peng, Y.B., Cui, J.X., Gu, H.T., Xu, L.Y., Li, Y.Q., Xu, Z.H., and Bai, S.N.
790 (2004). Developmental analyses reveal early arrests of the spore-bearing parts of
791 reproductive organs in unisexual flowers of cucumber (Cucumis sativus L.). Planta *220*,
792 230-240.
793 43. Edgar, B.A., and Orr-Weaver, T.L. (2001). Endoreplication cell cycles: More for less.
794 Cell *105*, 297-306.
795 44. De Veylder, L., Beeckman, T., Beemster, G.T.S., Engler, J.D., Ormenese, S., Maes, S.,
796 Naudts, M., Van der Schueren, E., Jacqmard, A., Engler, G., et al. (2002). Control of
797 proliferation, endoreduplication and differentiation by the Arabidopsis E2Fa-DPa
798 transcription factor. Embo J *21*, 1360-1368.

45. Gutierrez, C., Ramirez-Parra, E., Castellano, M.M., and del Pozo, J.C. (2002). G(1) to S transition: more than a cell cycle engine switch. Curr Opin Plant Biol *5*, 480-486.

46. Harbour, J.W., and Dean, D.C. (2000). The Rb/E2F pathway: expanding roles and emerging paradigms. Gene Dev *14*, 2393-2409.

47. Ramirez-Parra, E., Lopez-Matas, M.A., Frundt, C., and Gutierrez, C. (2004). Role of an atypical E2F transcription factor in the control of arabidopsis cell growth and differentiation. Plant Cell *16*, 2350-2363.

48. Jegu, T., Veluchamy, A., Ramirez-Prado, J.S., Rizzi-Paillet, C., Perez, M., Lhomme, A., Latrasse, D., Coleno, E., Vicaire, S., Legras, S., et al. (2017). The Arabidopsis SWI/SNF protein BAF60 mediates seedling growth control by modulating DNA accessibility. Genome Biol *18,* 114.

49. Cheniclet, C., Rong, W.Y., Causse, M., Frangne, N., Bolling, L., Carde, J.P., and Renaudin, J.P. (2005). Cell expansion and endoreduplication show a large genetic variability in pericarp and contribute strongly to tomato fruit growth. Plant Physiol *139*, 1984-1994.

50. Mauxion, J.P., Chevalier, C., and Gonzalez, N. (2021). Complex cellular and molecular events determining fruit size. Trends in plant science *26*, 1023-1038.

51. Renaudin, J.P., Deluche, C., Cheniclet, C., Chevalier, C., and Frangne, N. (2017). Cell layer-specific patterns of cell division and cell expansion during fruit set and fruit growth in tomato pericarp. J Exp Bot *68*, 1613-1623.

52. Khan, N.A., Khan, M.I.R., Ferrante, A., and Poor, P. (2017). Editorial: Ethylene: A Key Regulatory Molecule in Plants. Front Plant Sci *8*, 1782.

821 53. Park, C., Lee, H.Y., and Yoon, G.M. (2021). The regulation of ACC synthase protein
822 turnover: a rapid route for modulating plant development and stress responses. Curr Opin
823 Plant Biol *63*, 102046.
824 54. Iqbal, N., Khan, N.A., Ferrante, A., Trivellini, A., Francini, A., and Khan, M.I.R. (2017).
825 Ethylene Role in Plant Growth, Development and Senescence: Interaction with Other
826 Phytohormones. Front Plant Sci *8*, 475.
827 55. Boualem, A., Troadec, C., Camps, C., Lemhemdi, A., Morin, H., Sari, M.A., Fraenkel-
828 Zagouri, R., Kovalski, I., Dogimont, C., Perl-Treves, R., et al. (2015). A cucurbit
829 androecy gene reveals how unisexual flowers develop and dioecy emerges. Science *350*,
830 688-691.
831 56. Boualem, A., Lemhemdi, A., Sari, M.A., Pignoly, S., Troadec, C., Abou Choucha, F.,
832 Solmaz, I., Sari, N., Dogimont, C., and Bendahmane, A. (2016). The Andromonoecious
833 Sex Determination Gene Predates the Separation of Cucumis and Citrullus Genera. PloS
834 one *11,* e0155444.
835 57. Kirkbride, J.H. (1993). Biosystematic monograph of the genus *Cucumis* (Cucurbitaceae).
836 (North Carolina: Parkway Publishers).
837 58. Miller, J.S., and Diggle, P.K. (2003). Diversification of andromonoecy in Solanum
838 section Lasiocarpa (Solanaceae): the roles of phenotypic plasticity and architecture.
839 American Journal of Botany *90*, 707-715.
840 59. Loyd, D.G. (1980). Sexual strategies in plants. I. An hypothesis of serial adjustment of
841 maternal investment during one reproductive session. New Phytologist *86*, 69-79.
842 60. Bertin, R.I. (1982). The evolution and maintenance of andromonoecy. Evolutionary
843 Theory *6*, 25-32.

61. Vallejo-Marin, M., and Rausher, M.D. (2007). The role of male flowers in andromonoecious species: energetic costs and siring success in Solanum carolinense L. Evolution Int J Org Evolution *61*, 404-412.

62. Pereira, L., Ruggieri, V., Pérez, S., Alexiou, K.G., Fernández, M., Jahrmann, T., Pujol, M., and Garcia-Mas, J. (2018). QTL mapping of melon fruit quality traits using a high-density GBS-based genetic map. BMC Plant Biology *18,* 324.

63. Lazzaro, M.D., Wu, S., Snouffer, A., Wang, Y., and van der Knaap, E. (2018). Plant Organ Shapes Are Regulated by Protein Interactions and Associations With Microtubules. Front Plant Sci *9*, 1766.

64. Marchant, H.J. (1979). Microtubules, Cell-Wall Deposition and the Determination of Plant-Cell Shape. Nature *278*, 167-168.

65. Shibaoka, H. (1994). Plant Hormone-Induced Changes in the Orientation of Cortical Microtubules - Alterations in the Cross-Linking between Microtubules and the Plasma-Membrane. Annu Rev Plant Phys *45*, 527-544.

66. Roberts, I.N., Lloyd, C.W., and Roberts, K. (1985). Ethylene-Induced Microtubule Reorientations - Mediation by Helical Arrays. Planta *164*, 439-447.

67. Drevensek, S., Goussot, M., Duroc, Y., Christodoulidou, A., Steyaert, S., Schaefer, E., Duvernois, E., Grandjean, O., Vantard, M., Bouchez, D., et al. (2012). The Arabidopsis TRM1-TON1 Interaction Reveals a Recruitment Network Common to Plant Cortical Microtubule Arrays and Eukaryotic Centrosomes. Plant Cell *24*, 178-191.

68. Azimzadeh, J., Nacry, P., Christodoulidou, A., Drevensek, S., Camilleri, C., Amiour, N., Parcy, F., Pastuglia, M., and Bouchez, D. (2008). Arabidopsis TONNEAU1 proteins are

essential for preprophase band formation and interact with centrin. Plant Cell *20*, 2146-2159.

69. Spinner, L., Gadeyne, A., Belcram, K., Goussot, M., Moison, M., Duroc, Y., Eeckhout, D., De Winne, N., Schaefer, E., Van de Slijke, E., et al. (2013). A protein phosphatase 2A complex spatially controls plant cell division. Nat Commun *4,* 1863.

70. Xanthopoulou, A., Montero-Pau, J., Mellidou, I., Kissoudis, C., Blanca, J., Pico, B., Tsaballa, A., Tsaliki, E., Dalakouras, A., Paris, H.S., et al. (2019). Whole-genome resequencing of Cucurbita pepo morphotypes to discover genomic variants associated with morphology and horticulturally valuable traits. Hortic Res *6,* 94.

71. Colle, M., Weng, Y.Q., Kang, Y.Y., Ophir, R., Sherman, A., and Grumet, R. (2017). Variation in cucumber (Cucumis sativus L.) fruit size and shape results from multiple components acting pre-anthesis and post-pollination. Planta *246*, 641-658.

72. Lee, Y.K., Kim, G.T., Kim, I.J., Park, J., Kwak, S.S., Choi, G., and Chung, W.I. (2006). LONGIFOLIA1 and LONGIFOLIA2, two homologous genes, regulate longitudinal cell elongation in Arabidopsis. Development *133*, 4305-4314.

73. Nebenfuhr, A., and Dixit, R. (2018). Kinesins and Myosins: Molecular Motors that Coordinate Cellular Functions in Plants. Annu Rev Plant Biol *69*, 329-361.

74. Ookawara, R., Satoh, S., Yoshioka, T., and Ishizawa, K. (2005). Expression of alpha-expansin and xyloglucan endotransglucosylase/hydrolase genes associated with shoot elongation enhanced by anoxia, ethylene and carbon dioxide in arrowhead (Sagittaria pygmaea Miq.) tubers. Ann Bot-London *96*, 693-702.

75. Singh, A.P., Dubey, S., Lakhwani, D., Pandey, S.P., Khan, K., Dwivedi, U.N., Nath, P., and Sane, A.P. (2013). Differential expression of several xyloglucan

889 endotransglucosylase/hydrolase genes regulates flower opening and petal abscission in
890 roses. Aob Plants *5,* plt030.
891 76. Zhu, Q.G., Zhang, Z.K., Rao, J.P., Huber, D.J., Lv, J.Y., Hou, Y.L., and Song, K.H.
892 (2013). Identification of xyloglucan endotransglucosylase/hydrolase genes (XTHs) and
893 their expression in persimmon fruit as influenced by 1-methylcyclopropene and
894 gibberellic acid during storage at ambient temperature. Food Chem *138*, 471-477.
895 77. Smulders, M.J.M., and Horton, R.F. (1991). Ethylene Promotes Elongation Growth and
896 Auxin Promotes Radial Growth in Ranunculus-Sceleratus Petioles. Plant Physiol *96*, 806-
897 811.
898 78. Dahmani-Mardas, F., Troadec, C., Boualem, A., Leveque, S., Alsadon, A.A., Aldoss,
899 A.A., Dogimont, C., and Bendahmane, A. (2010). Engineering Melon Plants with
900 Improved Fruit Shelf Life Using the TILLING Approach. PloS one *5,* e15776.
901 79. Boualem, A., Fleurier, S., Troadec, C., Audigier, P., Kumar, A.P.K., Chatterjee, M.,
902 Alsadon, A.A., Sadder, M.T., Wahb-Allah, M.A., Al-Doss, A.A., et al. (2014).
903 Development of a Cucumis sativus TILLinG Platform for Forward and Reverse Genetics.
904 PloS one *9,* e97963.
905 80. Garcia-Mas, J., Benjak, A., Sanseverino, W., Bourgeois, M., Mir, G., Gonzalez, V.M.,
906 Henaff, E., Camara, F., Cozzuto, L., Lowy, E., et al. (2012). The genome of melon
907 (Cucumis melo L.). P Natl Acad Sci USA *109*, 11872-11877.
908 81. Huai, Q., Xia, Y., Chen, Y., Callahan, B., Li, N., and Ke, H. (2001). Crystal structures of
909 1-aminocyclopropane-1-carboxylate (ACC) synthase in complex with
910 aminoethoxyvinylglycine and pyridoxal-5'-phosphate provide new insight into catalytic
911 mechanisms. J Biol Chem *276*, 38210-38216.

82. Pedroza-Garcia, J.A., Domenichini, S., Mazubert, C., Bourge, M., White, C., Hudik, E., Bounon, R., Tariq, Z., Delannoy, E., del Olmo, I., et al. (2016). Role of the Polymerase is an element of sub-unit DPB2 in DNA replication, cell cycle regulation and DNA damage response in Arabidopsis. Nucleic Acids Res *44*, 7251-7266.

83. Tyanova, S., and Cox, J. (2018). Perseus: A Bioinformatics Platform for Integrative Analysis of Proteomics Data in Cancer Research. Methods Mol Biol *1711*, 133-148.

84. Tian, T., Liu, Y., Yan, H.Y., You, Q., Yi, X., Du, Z., Xu, W.Y., and Su, Z. (2017). agriGO v2.0: a GO analysis toolkit for the agricultural community, 2017 update. Nucleic Acids Res *45*, W122-W129.

85. Eleblu, J.S.Y., Haraghi, A., Mania, B., Camps, C., Rashid, D., Morin, H., Dogimont, C., Boualem, A., and Bendahmane, A. (2019). The gynoecious CmWIP1 transcription factor interacts with CmbZIP48 to inhibit carpel development. Sci Rep *9,* 15443.

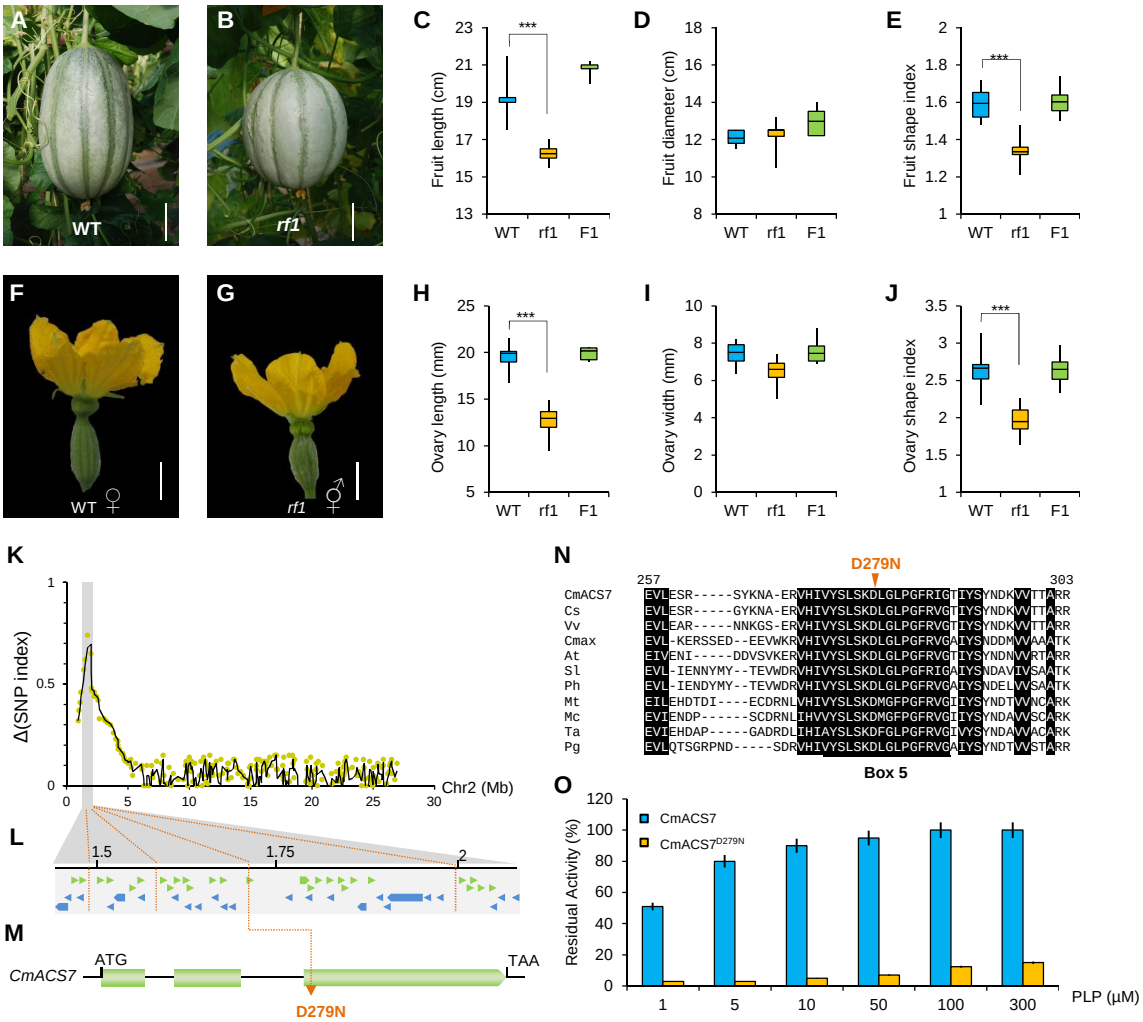
A
WT
B
rf1
C
Fruit length (cm)
***
WT rf1 F1
D
Fruit diameter (cm)
WT rf1 F1
E
Fruit shape index
***
WT rf1 F1
F
WT ♀
G
rf1 ♂
H
Ovary length (mm)
***
WT rf1 F1
I
Ovary width (mm)
WT rf1 F1
J
Ovary shape index
***
WT rf1 F1
K
Δ(SNP index)
Chr2 (Mb)
L
1.5
1.75
2
M
CmACS7
ATG
TAA
D279N
N
D279N
257
303
CmACS7 EVLESR-----SYKNA-ERVHIVYSLSKDLGLPGFRIGTIYSYNDKVVTTARR
Cs EVLESR-----GYKNA-ERVHIVYSLSKDLGLPGFRVGTIYSYNDKVVTTARR
Vv EVLEAR-----NNKGS-ERVHIVYSLSKDLGLPGFRVGTIYSYNDKVVTTARR
Cmax EVL-KERSSED--EEVWKRVHIVYSLSKDLGLPGFRVGAIYSNDDMVVAATK
At EIVENI-----DDVSVKERVHIVYSLSKDLGLPGFRVGTIYSYNDNVVRTARR
Sl EVL-IENNYMY--TEVWDRVHIVYSLSKDLGLPGFRIGAIYSNDAVIVSAATK
Ph EVL-IENDYMY--TEVWDRVHIVYSLSKDLGLPGFRVGAIYSNDELVVSAATK
Mt EILEHDTDI----ECDRNLVHIVYSLSKDMGFPGFRVGTIYSYNDTVVNCARK
Mc EVIENDP------SCDRNLIHVVYSLSKDMGFPGFRVGTIYSYNDAVVSCARK
Ta EVIEHDAP-----GADRDLIHIAYSLSKDFGLPGFRVGAVYSYNDAVVACARK
Pg EVLQTSGRPND-----SDRVHIVYSLSKDLGLPGFRVGAIYSYNDTVVSTARR
Box 5
O
Residual Activity (%)
CmACS7
CmACS7D279N
PLP (μM)

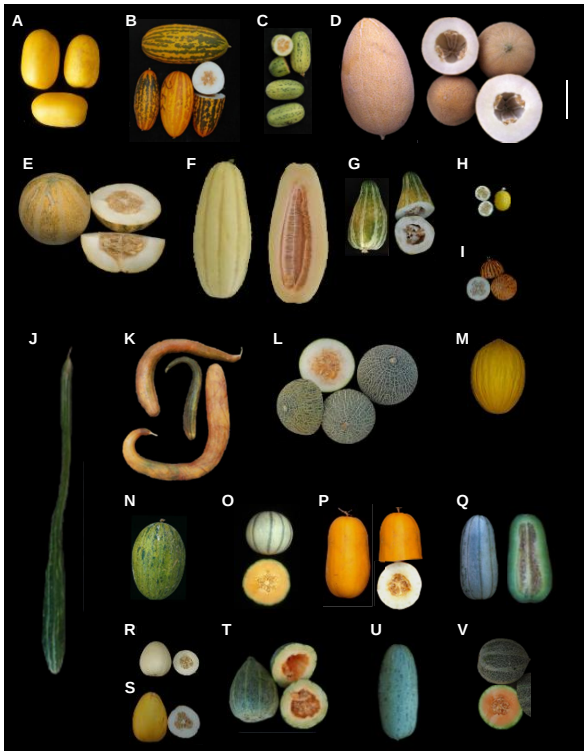
A
B
C
D
E
F
G
H
I
J
K
L
M
N
O
P
Q
R
S
T
U
V

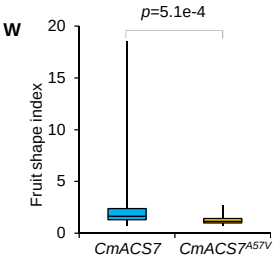
W
p=5.1e-4
Fruit shape index
20
15
10
5
0
CmACS7
CmACS7A57V

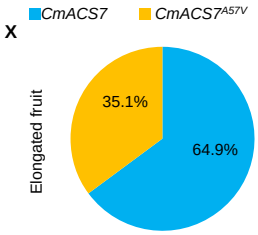
X
CmACS7
CmACS7A57V
Elongated fruit
35.1%
64.9%

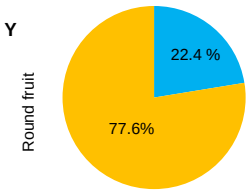
Y
Round fruit
22.4 %
77.6%

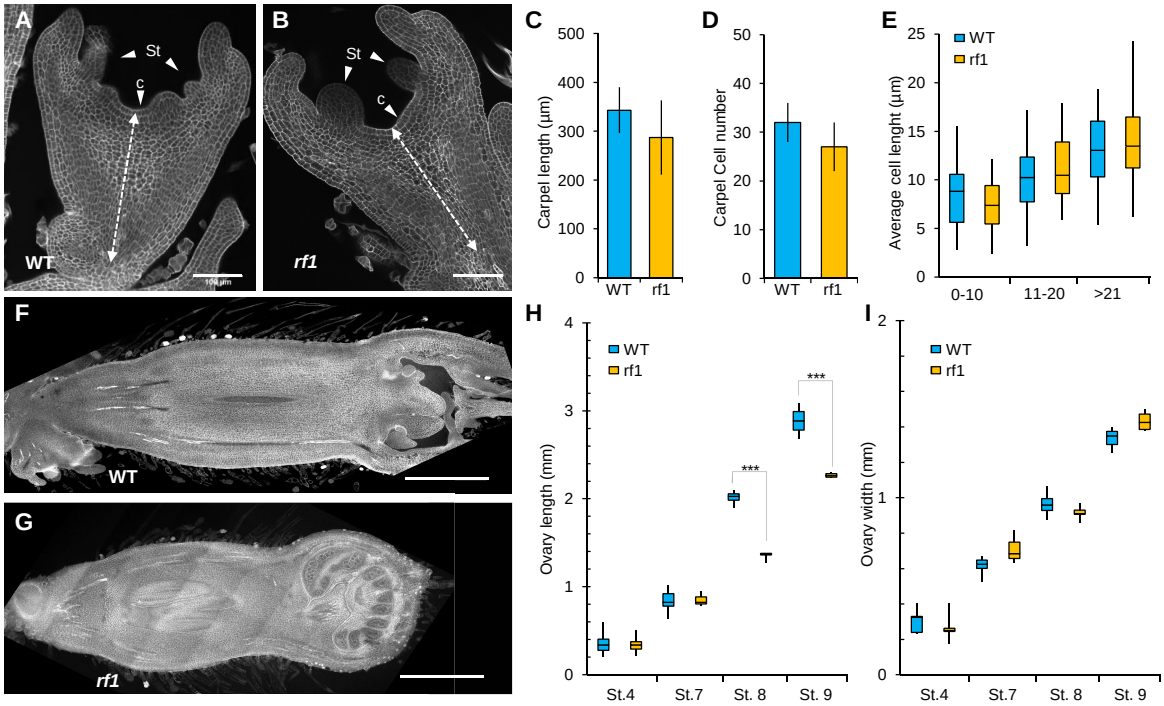
A
St
c
WT
B
St
c
rf1
C
Carpel length (µm)
500
400
300
200
100
0
WT
rf1
D
Carpel Cell number
50
40
30
20
10
0
WT
rf1
E
WT
rf1
Average cell lenght (µm)
25
20
15
10
5
0
0-10
11-20
>21
F
WT
G
rf1
H
WT
rf1
Ovary length (mm)
4
3
2
1
0
***
***
St.4
St.7
St. 8
St. 9
I
WT
rf1
Ovary width (mm)
2
1
0
St.4
St.7
St. 8
St. 9

A

	WT	*rf1*	*p-value*
ovary length (µm)	**1962 ± 87**	1340 ± 24	3.94 *e*-5
cell number in the longitudinal axis	144 ± 8	135 ± 5	ns
average cell length (µm)	**13.6 ± 0.6**	10.1 ± 0.5	1.26 *e*-5
ovary width (µm)	891± 68	920 ± 23	n.s
cell number in the transversal axis	94 ± 9	**117 ± 9**	0.003
average cell width (µm)	**9.5 ± 0.5**	7.8 ± 0.4	5.9 *e*-4
ovary shape index	**2.21 ± 0.2**	1.5 ± 0.03	5.8 *e*-4
cell shape index	**1.44 ± 0.1**	1.3 ± 0.09	0.026

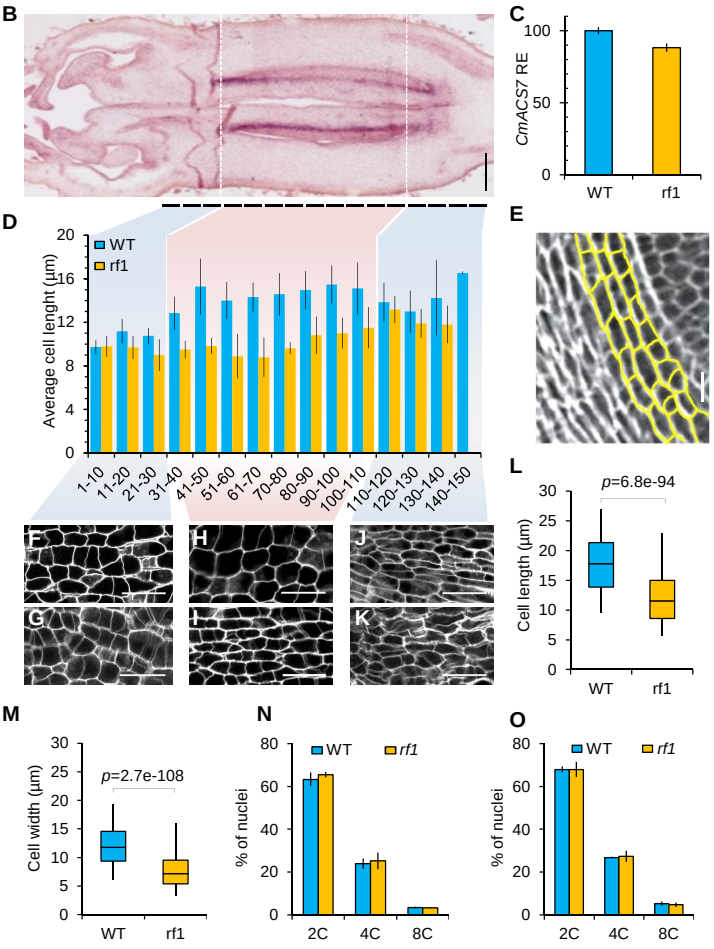

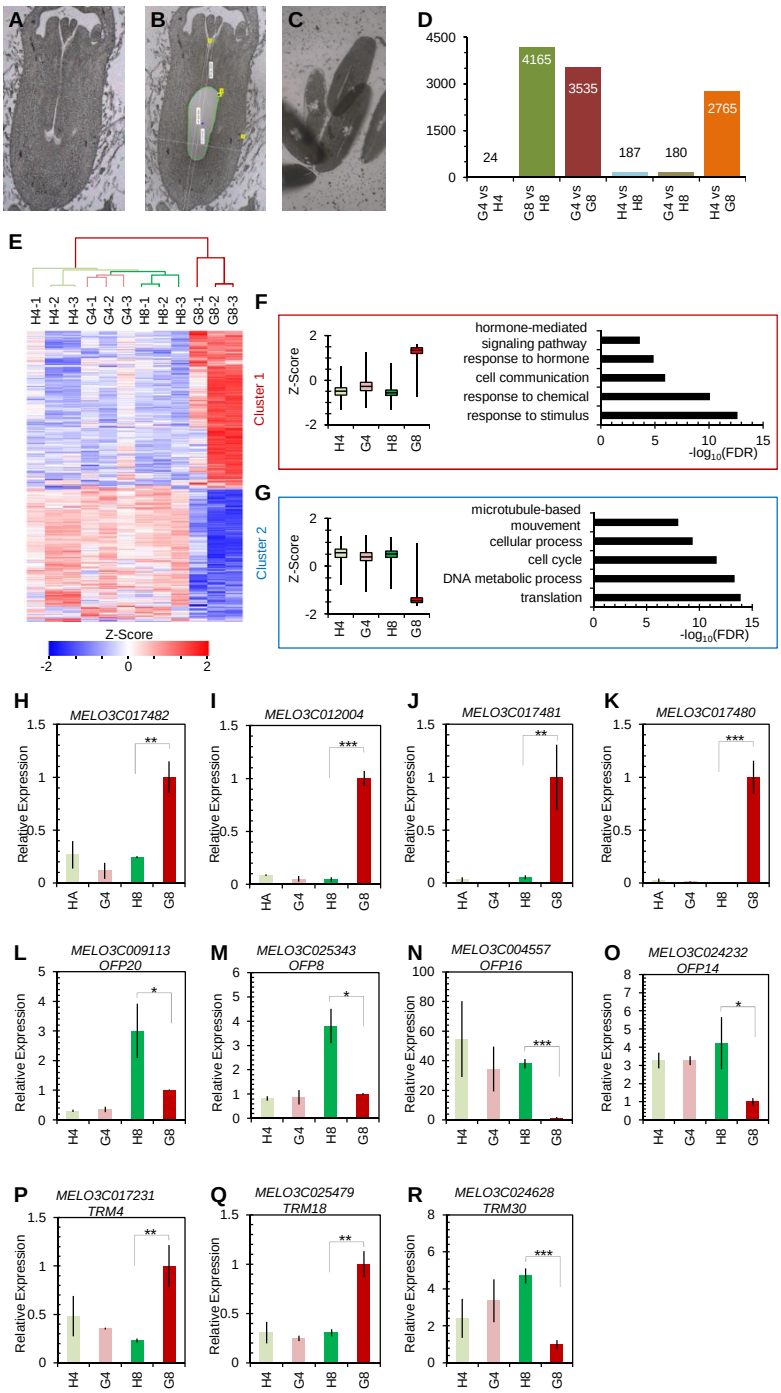
A
B
C
D
4500
3000
1500
0
24
4165
3535
187
180
2765
G4 vs H4
G8 vs H8
G4 vs G8
H4 vs H8
G4 vs H8
H4 vs G8
E
H4-1
H4-2
H4-3
G4-1
G4-2
G4-3
H8-1
H8-2
H8-3
G8-1
G8-2
G8-3
Z-Score
-2
0
2
F
Cluster 1
Z-Score
H4
G4
H8
G8
hormone-mediated signaling pathway
response to hormone
cell communication
response to chemical
response to stimulus
-log10(FDR)
G
Cluster 2
microtubule-based mouvement
cellular process
cell cycle
DNA metabolic process
translation
H
MELO3C017482
I
MELO3C012004
J
MELO3C017481
K
MELO3C017480
Relative Expression
HA
L
MELO3C009113
OFP20
M
MELO3C025343
OFP8
N
MELO3C004557
OFP16
O
MELO3C024232
OFP14
P
MELO3C017231
TRM4
Q
MELO3C025479
TRM18
R
MELO3C024628
TRM30

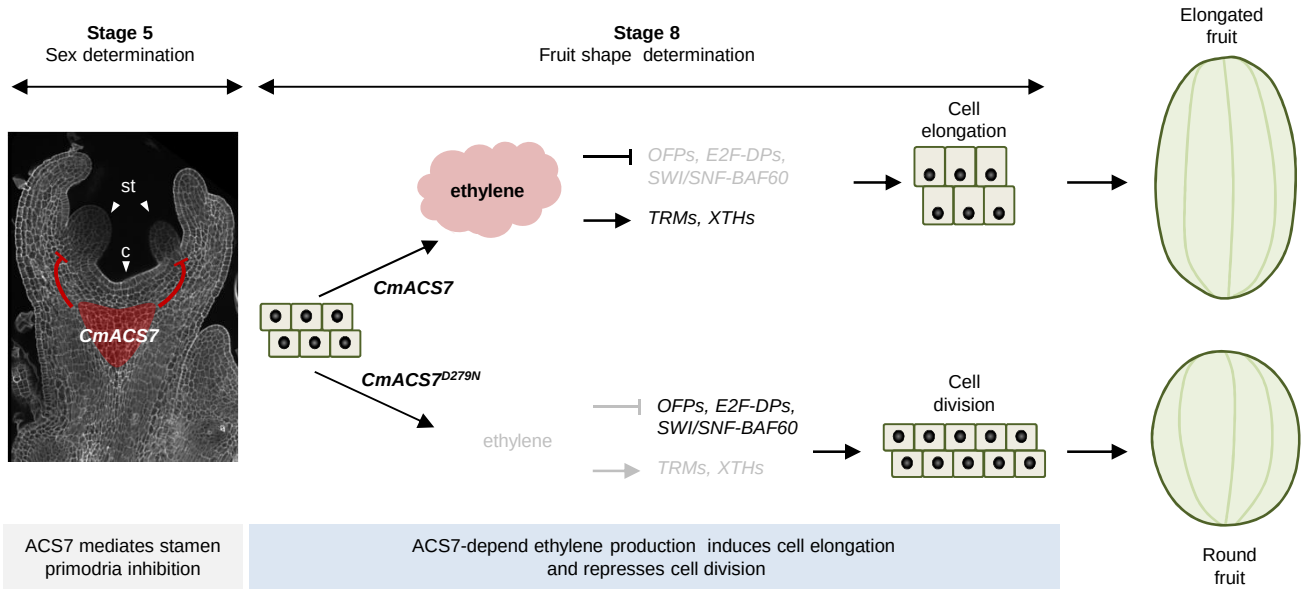
Stage 5
Sex determination
Stage 8
Fruit shape determination
Elongated fruit
st
c
CmACS7
ethylene
OFPs, E2F-DPs, SWI/SNF-BAF60
TRMs, XTHs
Cell elongation
CmACS7
CmACS7D279N
ethylene
OFPs, E2F-DPs, SWI/SNF-BAF60
TRMs, XTHs
Cell division
Round fruit
ACS7 mediates stamen primodria inhibition
ACS7-depend ethylene production induces cell elongation and represses cell division

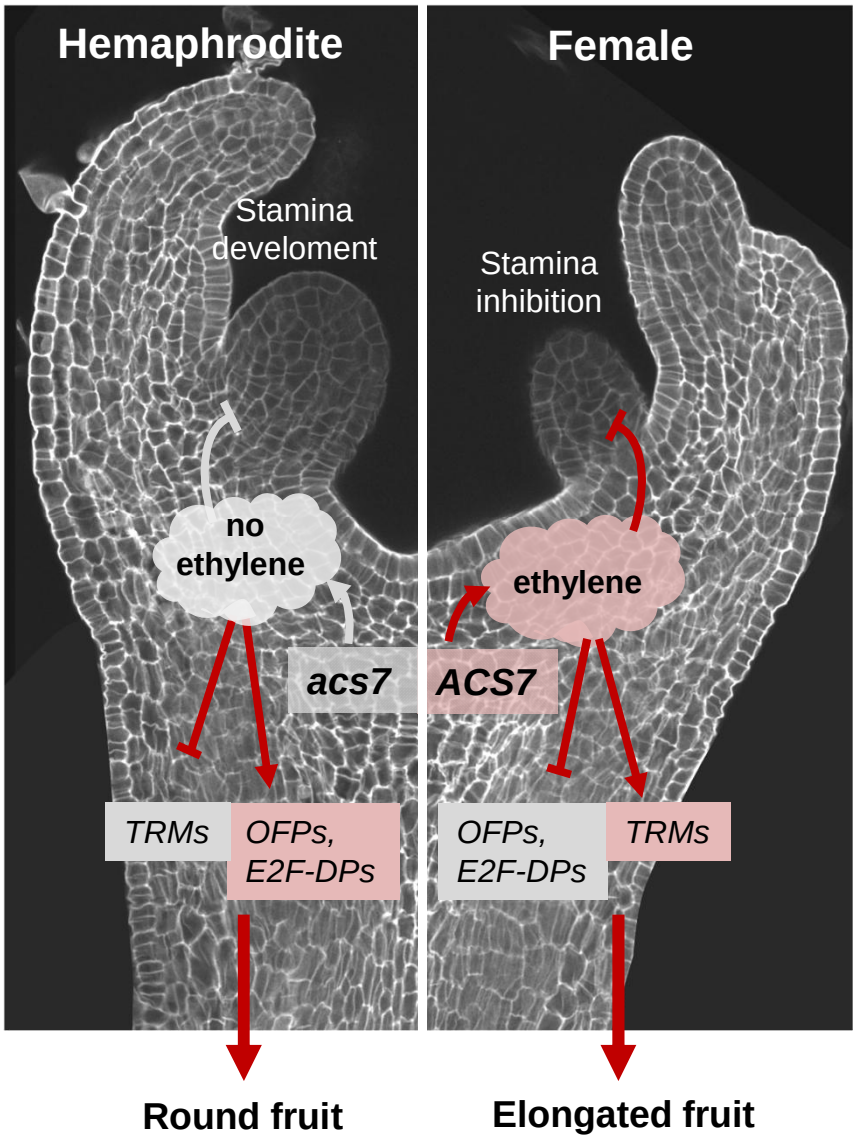
Hemaphrodite
Female
Stamina
develoment
Stamina
inhibition
no
ethylene
ethylene
acs7
ACS7
TRMs
OFPs,
E2F-DPs
OFPs,
E2F-DPs
TRMs
Round fruit
Elongated fruit